Correction of Ocular Artifacts in the EEG Using Bayesian Adaptive Regression Splines

Garrick L. Wallstrom
Robert E. Kass
Anita Miller
Jeffrey F. Cohn
Nathan A. Fox

ABSTRACT Ocular activity is a significant source of artifacts in the electroencephalogram (EEG). Regression upon the electrooculogram (EOG) is commonly used to correct the EEG. It is known, however, that this approach also removes high-frequency cerebral activity from the EEG. To counter this effect, we used Bayesian Adaptive Regression Splines (BARS) (DiMatteo (2001); DiMatteo, Genovese, and Kass (2001)) to adaptively filter the EOG of high-frequency activity before using the EOG for correction. In a preliminary simulation study, this approach reduced spectral error rates in higher frequency bands.

1 Introduction

The electroencephalogram (EEG) is an inexpensive, non-invasive method of measuring cerebral activity. Numerous scalp electrodes are used to record the low voltage electrical signals produced by neural populations. As a signal, the EEG is noisy and is contaminated by artifacts, potentials of non-cerebral origin. Ocular activity is a significant source of artifacts(Fisch(1991)). To help identify ocular artifacts, the electrooculogram (EOG) may be used. It uses electrodes placed in specific locations about the eyes to measure ocular activity (see Figure 1). As discussed in the section that follows, it is important to be able to filter (smooth) the EOG without distorting the signal. Filtering is extremely delicate because of the abrupt changes that appear simultaneously in the EOG and EEG (see Figure 2).

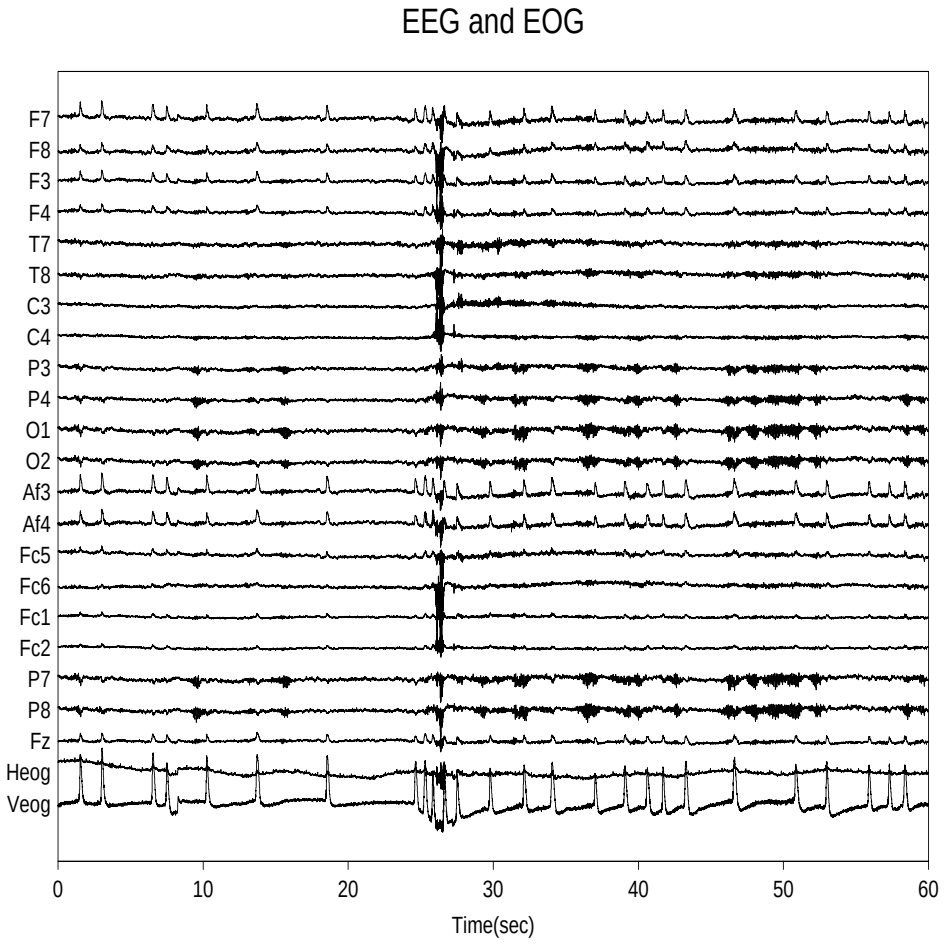

FIGURE 1. An example of EEG and EOG data. 21 channels of EEG and 2 EOG channels are displayed. The numerous spikes seen in some channels (most predominantly in F7,F8,F3,F4,Af3,and Af4) were caused by the blinking of the subject. Observe that the spikes also appear in the vertical EOG channel (VEOG).

This paper is a case study of Bayesian adaptive regression splines (BARS) (DiMatteo(2001), DiMatteo et al.(2001)), a new Bayesian method of fitting free-knot splines. In this application, BARS is successful at estimating the inhomogeneously smooth underlying ocular artifact. More details and discussion, oriented toward psychophysiologists, can be found in Wallstrom et al.(2001).

Section 2 provides background on the removal of ocular artifacts. In Section 3, we describe how regression is used to correct the EEG. In Section 4, we briefly discuss BARS. Sections 5 and 6 describe a simulation study of the effectiveness of BARS in this application. A discussion follows in Section 7.

2 Background on Ocular Artifact Removal

A variety of methods have been proposed for the handling of ocular artifacts (for a review see Croft and Barry(2000)). One common approach is artifact rejection. Manual ocular artifact rejection requires an individual to visually scan through the EEG data in search of artifacts. Sections of the data that are contaminated by artifacts are simply removed and not used in the analysis. There are several drawbacks to using artifact rejection. First, it can be very laborious and time consuming. Second, artifact rejection often results in a large loss in the amount of data available for analysis. Third, interesting changes in the pattern of EEG activity may occur simultaneously with eye movements, especially in event-related potential (ERP) and event-related dysynchronization (ERD) investigations. The first drawback can be addressed by using an automatic rejection method based on rejecting epochs where a voltage threshold is exceeded in the electrooculogram (EOG) or EEG channels. It is clear that the threshold controls the tradeoff between excessive rejection of artifact-free epochs and the false acceptance of epochs containing artifacts. Hence, the automatic rejection approach may save considerable resources, but at the expense of excessive data loss, failure to remove significant ocular artifacts, or both. Furthermore, even if the automatic method rejects perfectly, the second and third drawbacks to rejection still stand.

The alternative approach is to correct for ocular artifacts within some epochs, and reject epochs deemed incorrigible. Numerous methods for correction have been proposed. Some of these methods may be easily automated while others require considerable manual guidance. One large class of methods that can be easily automated is based on regressing out the EOG from the EEG. Both time domain (McCallum and Walter(1968), Hillyard and Galambos(1970), Quilter et al.(1977), Gratton et al.(1983)) and frequency domain (Whitton et al.(1978), Woestenburg et al.(1983), Gasser et al.(1985)) approaches have been used, although the benefit of

using frequency domain regression for ocular artifact correction has yet to be established (Brunia et al.(1989), Kenemans et al.(1991)). Other artifact correction methods are based on various multivariate methods such as principal components analysis(Lins et al.(1993b) and Lagerlund et al.(1997)) and independent components analysis(Jung et al.(2000)). In this paper we focus on the use of regression in the time domain.

One concern often raised regarding the use of regression for correction is the inability to account for bidirectional contamination. If ocular potentials can contaminate recordings by the EEG leads, then cerebral potentials can also contaminate recordings by the EOG leads. Therefore, regressing out the EOG from the EEG may not only remove ocular artifacts but may also remove interesting cerebral activity. Lins et al.(1993b) discuss the use of EOG filtering to partially combat this problem. Specifically, one may consider that the EOG is used twice in the process: once when the regression coefficients are calculated, and a second time when the weighted EOG is subtracted from the EEG. Lins et al.(1993b) stress that contamination of the EOG by cerebral potentials affects both uses of the EOG. They suggest that filtering the EOG prior to calculation of the coefficients addresses the contamination concern in the first instance. However, they use the unfiltered EOG in the second instance so, as they point out, the contamination concern remains. Intuitively, this concern could be overcome by the use of the filtered EOG in both instances. The problem is that the method of filtering is now of paramount importance. In order for regression using the filtered EOG to be effective for artifact correction the filtered EOG must not distort the ocular artifact. For example, a moving average filter may distort not only the shape of the artifact, but also the temporal characteristics of the artifact. Both features of the artifact must be retained in order for regression to be successful removing the artifact from the EEG. In this paper we use Bayesian adaptive regression splines to filter the EOG as they are able to remove high frequency activity while not distorting the essential features of the artifact.

3 Artifact Correction via Regression

It has been noted (Corby and Kopell(1972), Gratton et al.(1983), Lins et al.(1993a)), that the strength of the contribution of ocular activity to the EEG can depend on the type of artifact present. This difference in the regression coefficients is due to the artifacts being generated by different sources. Since the regression approach is not spatial, regression is unable to account for multiple artifacts with distinct generators. Therefore very short epochs should be used so that, at least approximately, only one type of artifact, or one combination of artifacts, is present throughout the epoch. Within an epoch, each channel of EEG and EOG is centered to have zero-

mean before regression is used.

The following linear model is used as an approximation to the relationship between the m channels of observed EOG, the observed EEG and the true unobserved EEG, where by 'true' EEG, we mean the signal that would have been recorded in the absence of ocular artifacts.

$$\mathrm{OBS}_i(t) = \sum_{j=1}^{m} \alpha_{ij} F(\mathrm{EOG}_j)(t) + \mathrm{EEG}_i(t),$$

where $\mathrm{OBS}_i(t)$ denotes the observed EEG recording from lead i at time t, EOG_j denotes the observed recording from the jth EOG channel, and $\mathrm{EEG}_i(t)$ denotes the true unobserved EEG from lead i at time t. In the above equation, $F(\cdot)$ denotes a filter.

Multiple regression may be used to estimate the values of α_{ij}. The estimated true EEG is then formed according to

$$\widehat{\mathrm{EEG}}_i(t) = \mathrm{OBS}_i(t) - \sum_{j=1}^{m} \widehat{\alpha}_{ij} F(\mathrm{EOG}_j)(t).$$

In our implementation, the correction procedures were applied to 1 second epochs (512 sample points) with 50% overlap throughout the realization. The overlap of epochs allows the corrected epochs to be combined into a single continuous corrected realization (see Appendix).

The first correction procedure uses the raw, unfiltered EOG channels in the regression. We refer to this correction procedure by REG-RAW. For the second correction procedure, which we refer to by REG-ADAPT, we adaptively filter the EOG realizations prior to correcting via regression. Details on the adaptive filter are given next.

4 Bayesian Adaptive Regression Splines

We employ Bayesian adaptive regression splines (BARS) (DiMatteo(2001),DiMatteo et al.(2001)) to adaptively filter the EOG. BARS smooths a scatterplot using splines with an unknown number of knots and knot locations. In this application, we used a model of the following form.

$$\begin{aligned}
\mathbf{Y}|k,\xi,\beta,\sigma &\sim N_n\left(\mathbf{B}\beta, \sigma^2 I\right) \\
\beta|k,\xi,\sigma &\sim N_{k+m}\left(0, \sigma^2 n \left(\mathbf{B}^T\mathbf{B}\right)^{-1}\right) \\
\pi(\sigma) &\propto \sigma^{-1} \\
\xi|k &\sim \text{Uniform} \\
k|\lambda &\sim \text{Poisson}(\lambda)
\end{aligned} \tag{1}$$

Here, Y is the observed EOG, k is the number of knots, ξ is the vector of knot locations and $\mathbf{B}$ is the mth order B-spline basis matrix. The above prior on β is called the *unit-information prior* by Kass and Wasserman(1995).

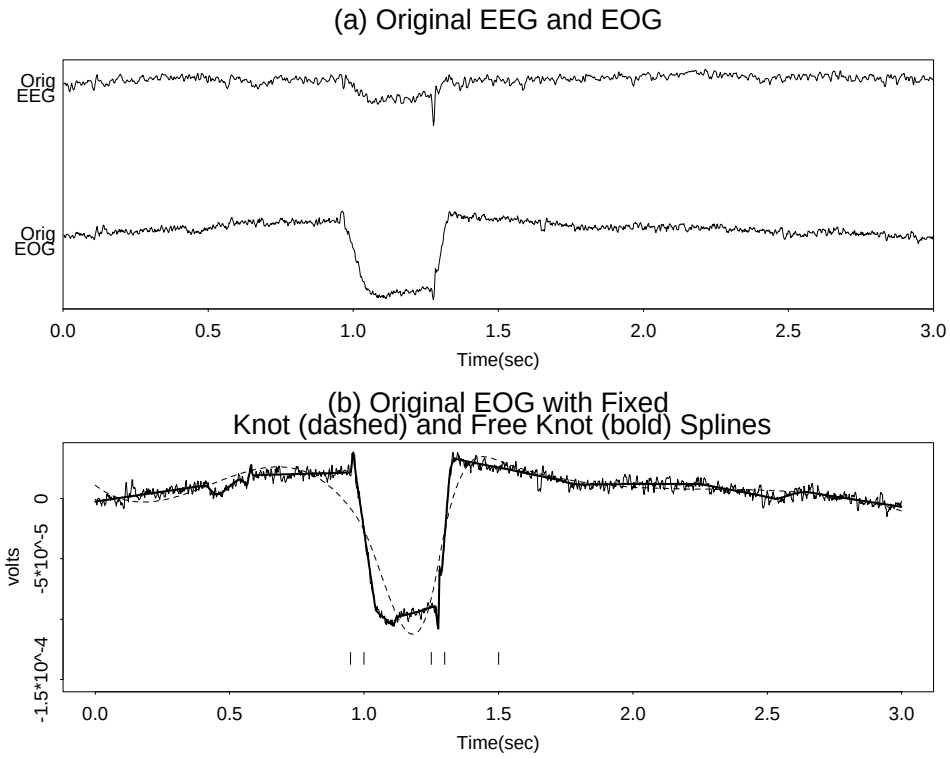

FIGURE 2. (a) A single channel of EEG and EOG are shown. (b) The unfiltered EOG with two smooths. The dashed line is a spline fit with knots fixed at 0.95,1,1.25,1.3 and 1.5, indicated in the plot with short vertical lines. These knot locations allow the spline to capture the general trend of the artifact, but important features of the artifact that are clearly present in the EEG have been lost. The bold line is the filtered EOG using BARS. It can be seen that the essential features of the artifact have been transferred to the BARS-filtered EOG unadulterated while the high frequency activity has been filtered out.

Reversible-jump Markov chain Monte Carlo (Green(1995)) is used to sample from the marginal posterior distribution of (k, ξ). There are three features of BARS that are worth pointing out. First, in the model above, analytical integration permits sampling from the marginal posterior of (k, ξ). With more general models, an approximation of a likelihood ratio by Kass and Wasserman(1995) facilitates sampling from the marginal posterior of (k, ξ) when the unit-information prior is used. Second, the posterior sim-

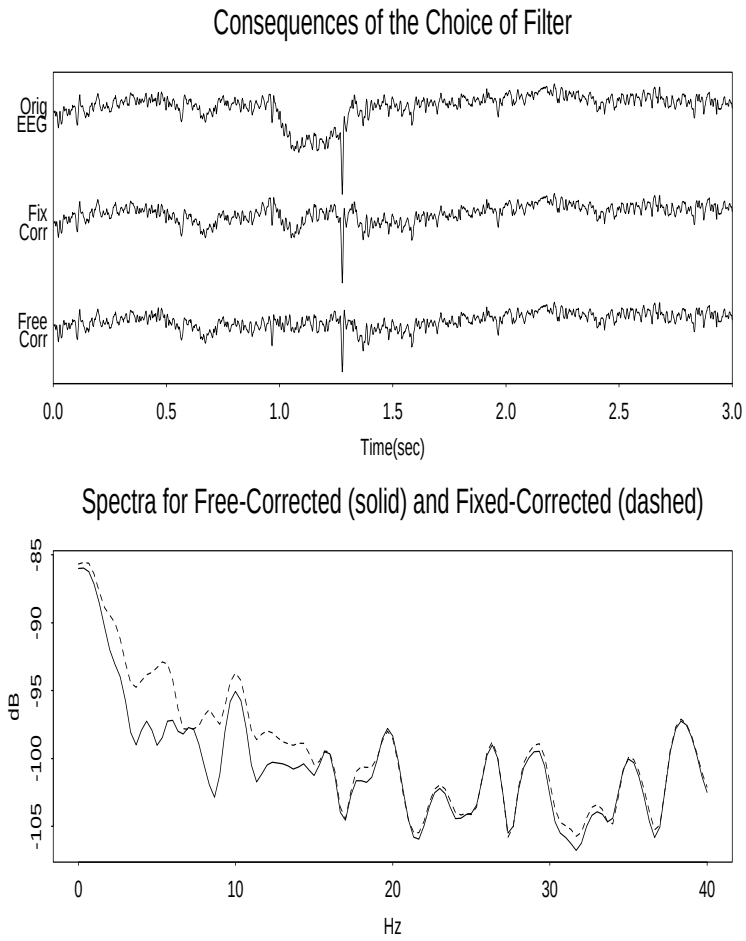

FIGURE 3. The consequences of the choice of filter. Top: The original EEG, the corrected EEG based on the fixed-knot spline shown in Figure 2, and the corrected EEG based on the free-knot spline fit using BARS. While neither is able to account for the large downward spike, the BARS fit is more successful at removing the artifact. Bottom: The spectra for the two corrections. The choice of filter has a large impact through 15 Hz.

ulation employs the locality heuristic suggested by Zhou and Shen(1998), by which new knots tend to be inserted near other knots. Third, credible statements may be easily generated from the posterior simulation.

In a simulation study (DiMatteo et al.(2001)) BARS outperformed the adaptive regression spline methods of Zhou and Shen(1998) and of Denison et al.(1998). Also, Zhou and Shen(1998) showed that their method (SARS) was superior to the wavelet method of Donoho and Johnstone(1995).

In the artifact correction context, knots should tend to be placed around

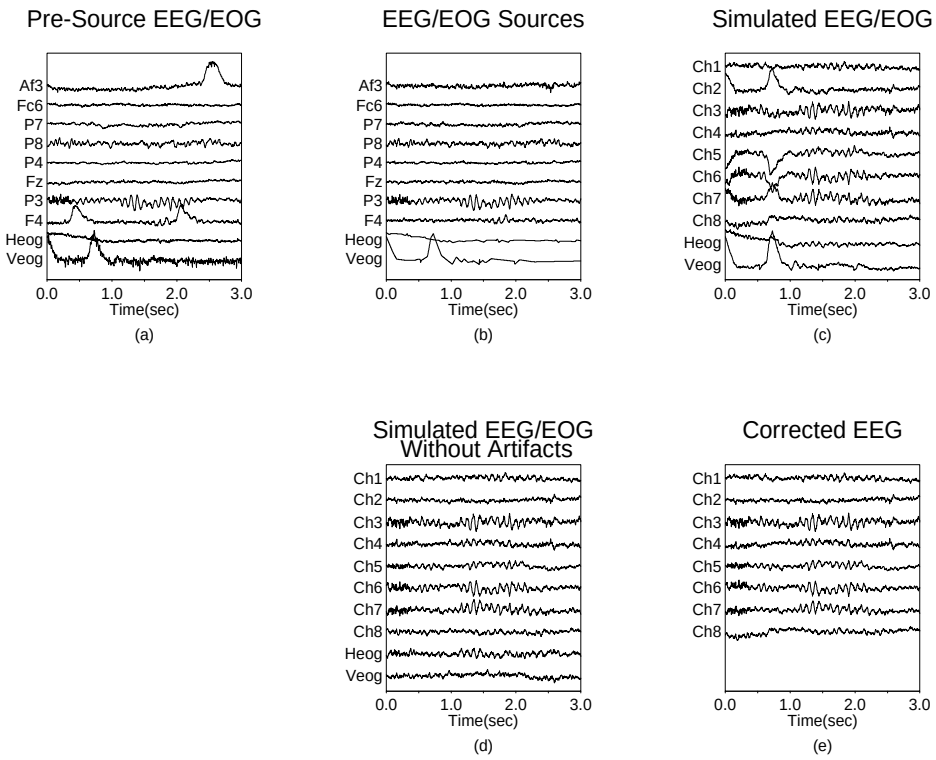

FIGURE 4. (a): Each pre-source channel originates from a different, randomly selected subject. The EEG pre-sources were randomly selected 3s epochs taken from randomly selected EEG channels. The EOG pre-sources were randomly selected 3s epochs taken from the corresponding EOG channels. (b): Each EEG source was derived from the corresponding EEG pre-source by applying an artifact correction procedure (REG-RAW). Each EOG source was derived from the corresponding EOG pre-source by applying the free-knot spline adaptive filter. (c): The simulated EEG/EOG was obtained by multiplying the EEG/EOG sources by a random weight matrix. (d) To simulate the EEG and EOG that would have been observed in the absence of artifacts, the EEG/EOG sources were multiplied by the same weight matrix, modified by replacing the EEG source coefficients with zeroes. (e) The corrected EEG was obtained by applying an artifact correction procedure to the simulated EEG/EOG. This corrected EEG was then compared to the EEG/EOG simulated without artifacts given in (d).

large amplitude artifacts, and few knots should be required in artifact-free regions. This adaptive quality permits filtering of the EOG without distortion of the shape and temporal features of the artifacts (see Figures 2 and 3). We chose to use second-order splines ($m = 2$) because the artifacts

often appear in the EOG (and particularly in the horizontal EOG channel) as sharp jumps, which are more easily fit using splines of lower order.

5 Simulation Method

In order to investigate the effect of the adaptive filter, we simulated 20 3-second epochs of EEG and EOG data. This section describes the simulation method used. It is based on real EEG and EOG data collected in an ongoing study of childhood-onset depression (Miller et al.(2000)).The real data consist of 60 second recordings of baseline EEG and EOG for 12 adult subjects under an eyes-open condition. Half of the subjects had a history of childhood-onset depression, and half had no history of major psychopathology. The EEG was collected from scalp electrodes positioned according to the expanded International 10-20 System. All sites were recorded using the vertex (Cz) reference. Two channels of EOG were used. The vertical EOG was recorded using two electrodes placed above and below the right eye. The horizontal EOG was recorded using two electrodes placed on the outer canthi. The sampling rate was 512 Hz.

The simulation process is diagrammed in Figure 4. For each epoch we began by simulating 10 independent potential sources, 8 cerebral, one horizontal ocular, and one vertical ocular. We then created a random mixing matrix to enable the construction of the observed and true EEG and EOG channels.

To simulate a 3 second realization of a cerebral source, we began by selecting a random 3 second segment of a randomly selected observed EEG channel for a randomly selected subject. We call this the pre-source EEG. We then simulated the EEG source by removing significant ocular artifacts from the pre-source via regression upon the unfiltered EOG (REG-RAW).

To simulate the two ocular sources, we formed pre-source EOG by selecting random 3 second segments of the observed EOG from randomly selected subjects. The EOG sources were then obtained by filtering the pre-source EOG using free knot splines. The ten subjects from which the EEG and EOG pre-sources were taken were selected randomly, without replacement, from among the 12 subjects in the available set of data. Since each channel of data was derived from a different subject, the ten channels are truly independent.

Note that, aside from the artifact removal, we have used independent segments of observed EEG as cerebral sources. While there is no guarantee that the true cerebral sources resemble the potentials recorded on the scalp, this use of the observed EEG helps ensure that the simulated scalp EEG resemble real EEG.

The observed EEG and EOG data are simulated by multiplying the simulated sources by a random weight matrix. The simulated observed chan-

nels are therefore linear combinations of the simulated cerebral and ocular sources. The EEG coefficient vectors are formed by normalizing vectors of independent standard normal random variates. The EOG coefficient vectors require additional care. Since each EOG is primarily a measure of ocular potentials, it is important that the two ocular sources are significant contributors to the observed EOG channels, respectively. This suggests heavily weighting the contribution from the corresponding ocular source. On the other hand, the observed EOG should contain a similar amount of noise as the observed EEG, suggesting that there should still be considerable non-ocular contributions. We therefore set the coefficient of the corresponding ocular source to be 1. The remaining coefficients are formed from independent standard normal random variates, scaled so that the squared norm of the remaining coefficients is 0.9. Therefore, for both EOG and EEG, the expected squared coefficient of a cerebral source is 0.1.

To evaluate the performance of the correction procedures, we need to create the true EEG that correspond to the simulated observed EEG. This can be accomplished by multiplying the simulated sources by the weight matrix formed above with the ocular source coefficients replaced with zeroes.

6 Simulation Results

To evaluate the artifact correction procedures we investigated errors in both the time and frequency domains. In the time domain, for each channel, we aligned the overlapping corrected 1 second epochs into a 3 second corrected realization. We then calculated the mean squared error between the true EEG and the corrected EEG. In the frequency domain, for each channel we estimate power density (in dB) for four frequency bands, delta (1.5 Hz to 3.5 Hz), theta (3.5 Hz to 7.5 Hz), alpha (7.5 Hz to 12.5 Hz) and beta (12.5 Hz to 19.5 Hz). Specifically, the EEG was average referenced and power was estimated using a Hanning window taper on 1 second epochs with 50% overlap. For each epoch and frequency band, power density was formed by averaging the power estimates for frequencies within the band. Average power density was then computed by averaging the power density over all overlapping epochs and converting to decibels. For each correction method, we computed power density errors for each channel and frequency band.

The time and frequency domain errors are summarized in Table 1.1. The first row of the table gives the mean square root of the mean squared error for the two correction methods. The remaining rows give the mean absolute error for power density expressed in decibels. The errors that result when no correction or rejection method is applied are also summarized. Two observations should be made. First, if we compare the mean errors from no correction to correction without filtering we see that, in the higher

	REG-ADAPT	REG-RAW	NO-CORR
Time Domain (μv)	3.73 (0.14)	4.38 (0.16)	9.72 (0.97)
Delta Band (dB)	1.48 (0.10)	1.52 (0.11)	5.02 (0.53)
Theta Band (dB)	1.14 (0.08)	1.21 (0.09)	3.35 (0.37)
Alpha Band (dB)	1.14 (0.11)	1.54 (0.14)	0.89 (0.14)
Beta Band (dB)	0.60 (0.05)	1.12 (0.09)	0.65 (0.09)

TABLE 1. Table of mean correction errors by method. Standard errors are given in parentheses. Each row displays the mean error for the two correction methods (REG-ADAPT and REG-RAW) and for no correction. The first row uses a time domain measure of error, the square root of the mean squared error. The second through fifth rows measure mean absolute error in terms of power within the delta (1.5 Hz to 3.5 Hz), theta (3.5 Hz to 7.5 Hz), alpha (7.5 Hz to 12.5 Hz) and beta (12.5 Hz to 19.5 Hz) bands respectively.

frequency bands (alpha and beta), correction without filtering is detrimental. Second, if we compare correction without filtering to correction with adaptive filtering, we see that there is improvement in the time domain and in the higher frequency bands. In the lower bands (delta and theta) the adaptive filtering had little effect, as expected.

7 Discussion

This study concerns the use of Bayesian adaptive regression splines to improve ocular artifact correction in the EEG. We argue that careful filtering of the EOG prior to correction should reduce bidirectional contamination between the EEG and the EOG. BARS is particularly well suited to this task since the underlying artifact is not homogeneously smooth. BARS is able to fit an inhomogeneously smooth function to the data by placing more knots in regions with less smoothness and fewer knots in regions with more smoothness. By doing so, it is able to remove the high frequency cerebral activity from the EOG while not distorting the essential characteristics of the artifact. The simulation study suggests that the use of BARS does reduce error rates in the higher frequency bands. Other methods of adaptive smoothing, such as wavelets, may also be successful in this context.

The biggest drawback to the use of BARS as an adaptive smoother is the computation time. We like BARS for the following reasons:

- It works well. In the simulation study of DiMatteo et al.(2001), BARS outperformed the free-knot spline methods of Zhou and Shen(1998) and of Denison et al.(1998).
- It generalizes easily. The model (4.1) could be easily replaced by a more general model, such as a generalized linear model.
- The posterior simulation permits the easy generation of credible curves. Inferences on functions of (k, ξ, β), such as the curve mode, can be made by including an additional step in the posterior simulation.

We direct the reader to DiMatteo et al.(2001) for further details and discussion of BARS. Wallstrom et al.(2001) contains a more in-depth discussion of the application to EEG artifact correction, geared for psychophysiologists.

Acknowledgements

Support for the current work was provided by NIMH Program Project MH56193, NSF VIGRE Award DMS-9819950, NIMH Postdoctoral Fellowship MH18951, NIMH Seed Award MH30915 and a NARSAD Young Investigator Award.

References

Brunia, C., Möcks, J., van den Berg-Lenssen, M., Coelho, M., Coles, M., Elbert, T., Gasser, T., Gratton, G., Ifeachor, E., Jervis, B., Lutzenberger, W., Sroka, L., van Blokland-Vogelesang, A., van Driel, G. and Woestenburg, J. (1989). Correcting ocular artifacts in the EEG: a comparison of several methods. *Journal of Psychophysiology* **3** 1–50.

Corby, J. and Kopell, B. (1972). Differential contributions of blinks and vertical eye movements as artifacts in EEG recording. *Psychophysiology* **3** 640–644.

Croft, R. and Barry, R. (2000). Removal of ocular artifact from the EEG: a review. *Neurophysiol Clin* **30** 5–19.

Denison, D., Mallick, M. and Smith, A. (1998). Automatic bayesian curve fitting. *JRSS Ser. B* **60** 333–350.

DiMatteo, I. (2001). *Bayesian curve-fitting with free-knot splines.* Ph.D. thesis, Department of Statistics, Carnegie Mellon University.

DiMatteo, I., Genovese, C. and Kass, R. (2001). Bayesian curve fitting with free-knot splines. To appear, Biometrika.

Donoho, D. and Johnstone, I. (1995). Adaptive to unknown smoothness via wavelet shrinkage. *JASA* **90** 1200–1224.

Fisch, B. (1991). Artifacts. In B. Fisch, ed., *Spehlmann's EEG Primer.* Elsevier, 2nd ed., 108–124.

Gasser, T., Sroka, L. and Möcks, J. (1985). The transfer of EOG activity into the EEG for eyes open and closed. *Electroencephalography and Clinical Neurophysiology* **61** 181–193.

Gratton, G., Coles, M. and Donchin, E. (1983). A new method for the off-line removal of ocular artifact. *Electroencephalography and Clinical Neurophysiology* **55** 468–484.

Green, P. (1995). Reversible jump markov chain monte carlo computation and bayesian model determination. *Biometrika* **82** 711–732.

Hillyard, S. and Galambos, R. (1970). Eye-movement artifact in the CNV. *Electroencephalography and Clinical Neurophysiology* **28** 173–182.

Jung, T.-P., Makeig, S., Humphries, C., Lee, T.-W., McKeown, M. J., Iragui, V. and Sejnowski, T. J. (2000). Removing electroencephalographic artifacts by blind source separation. *Psychophysiology* **37** 163–178.

Kass, R. and Wasserman, L. (1995). A reference bayesian test for nested hypotheses and its relationship to the schwarz criterion. *JASA* **90** 928–934.

Kenemans, J., Molenaar, P., Verbaten, M. and Slangen, J. (1991). Removal of the ocular artifact from the EEG: a comparison of time and frequency domain methods with simulated and real data. *Psychophysiology* **28** 114–121.

Lagerlund, T. D., Sharbrough, F. W. and Busacker, N. E. (1997). Spatial filtering of multichannel electroencephalographic recordings through principal component analysis by singular value decomposition. *Journal of Clinical Neurophysiology* **14** 73–82.

Lins, O. G., Picton, T. W., Berg, P. and Scherg, M. (1993a). Ocular artifacts in EEG and event-related potentials I: Scalp topography. *Brain Topography* **6** 51–63.

Lins, O. G., Picton, T. W., Berg, P. and Scherg, M. (1993b). Ocular artifacts in recording EEGs and event-related potentials II: Source dipoles and source components. *Brain Topography* **6** 65–78.

McCallum, W. and Walter, W. (1968). The effect of attention and distraction on the contingent negative variation in normal and neurotic subjects. *Electroencephalography and Clinical Neurophysiology* **25** 319–329.

Miller, A., Fox, N. A., Cohn, J. F., Forbes, E. E., Sherrill, J. T. and Kovacs, M. (2000). Regional patterns of brain activity in adults with a history of childhood-onset depression are influenced by sex differences, depressive subtypes, and comorbid psychopathology. Submitted to Archives of General Psychiatry.

Quilter, P., MacGillivray, B. and Wadbrook, D. (1977). The removal of eye movement artifact from EEG signals using correlation techniques. In *IEEE Conference on Random Signal Analysis. Conference publication* No. 159.

Wallstrom, G., Kass, R., Miller, A., Cohn, J. and Fox, N. (2001). Automatic correction of ocular artifacts in the EEG: A comparison of regression-based and component-based methods. Submitted.

Whitton, J., Lue, F. and Moldofsky, H. (1978). A spectral method for removing eye movement artifacts from the EEG. *Electroencephalography and Clinical Neurophysiology* **44** 735–741.

Woestenburg, J., Verbaten, M. and Slangen, J. (1983). The removal of the eye-movement artifact from the EEG by regression analysis in the frequency domain. *Biological Psychology* **16** 127–147.

Zhou, S. and Shen, X. (1998). Spatially adaptive regression splines and accurate knot selection schemes. Tech. rep., Department of Statistics, Ohio State University.

Appendix: Reconciling Overlapping Signals

A consequence of using a method that operates on small overlapping portions of an epoch is a need to reconcile the corrected portions at the end. This appendix describes the procedure we used. To simplify the discussion, for now suppose that there are two signals defined on overlapping epochs where each signal was formed by applying a correction method to the observed EEG channel. Let $S_1(t)$ denote the first signal, defined for $t_0 < t \leq t_2$, and $S_2(t)$ denote the second signal, defined for $t_1 < t \leq t_3$. We are interested in reconciling $S_1(t)$ and $S_2(t)$ for $t_1 < t \leq t_2$. As each of the correction methods discussed herein amount to subtracting a linear combination of the EEG and possibly filtered EOG channels, the difference between S_1 and S_2 in the overlap region is also a linear combination of the EEG and possibly filtered EOG channels. While the EEG and EOG are

centered prior to correction on each epoch, the channels need not have zero mean on the overlap portion of the epoch. It follows that in the overlap region, S_1 and S_2 are not mutually centered. Therefore the reconciliation procedure that we use contains two steps.

(i) Vertically shift S_2 so that S_1 and S_2 have the same center in the overlap region.

(ii) Form a single signal S such that in the overlap region S is a weighted average of S_1 and S_2.

For step (i), we simply define $S_2^*(t) = S_2(t) - m_2 + m_1$, where m_1 and m_2 are the respective means of S_1 and S_2 in the overlap region. For step (ii), let $w(x)$ be a continuous weight function defined for $0 \leq x \leq 1$ such that $w(0) = 0$ and $w(1) = 1$, and define

$$S(t) = \begin{cases} S_1(t), & t_0 < t \leq t_1 \\ S_1(t)\left[1 - w\left(\frac{t-t_1}{t_2-t_1}\right)\right] + S_2^*(t) w\left(\frac{t-t_1}{t_2-t_1}\right), & t_1 < t \leq t_2 \\ S_2^*(t). & t_2 < t \leq t_3 \end{cases}$$

The weight function is continuous with $w(0) = 0$ and $w(1) = 1$ to ensure that discontinuities are not introduced into S. We used $w(x) = x$ as a simple and obvious choice.

More generally, suppose we want to reconcile signals $S_1, \ldots, S_n$ where $S_j(t)$ is defined for $t_{j-1} < t \leq t_{j+1}$ and $t_0 < t_1 < \cdots < t_{n+1}$. Then for $j = 1, \ldots, n$ let l_j denote the mean of S_j over the interval $(t_{j-1}, t_j]$ and let h_j denote the mean of S_j over the interval $(t_j, t_{j+1}]$. Define $S_1^*(t) = S_1(t)$ and, for $j = 2, \ldots, n$ define $S_j^*(t) = S_j(t) - \sum_{i=2}^{j}(l_i - h_{i-1})$. Finally, the resulting signal is given by

$$S(t) = \begin{cases} S_1^*(t), & t_0 < t \leq t_1 \\ S_j^*(t)\left[1 - w\left(\frac{t-t_j}{t_{j+1}-t_j}\right)\right] + S_{j+1}^*(t) w\left(\frac{t-t_j}{t_{j+1}-t_j}\right), & t_j < t \leq t_{j+1}, \\ & j = 1, \ldots, n-1 \\ S_n^*(t), & t_n < t \leq t_{n+1} \end{cases}$$